Charles University

Faculty of Science

Study programme: Chemistry

Branch of Study: Medicinal Chemistry

Michal Kalus

Peak shape distortions in capillary electrophoresis

Bachelor's Thesis

Supervisor: Mgr. Magda Dovhunová

Consultant: Mgr. Pavel Dubský, Ph.D.

Prague, 2018

Prohlášení:

Prohlašuji, že jsem závěrečnou práci zpracoval samostatně a že jsem uvedl všechny použité informační zdroje a literaturu. Tato práce ani její podstatná část nebyla předložena k získání jiného nebo stejného akademického titulu.

V Praze, 2018

Michal Kalus

Declaration:

I declare that I did the final work independently and that I have provided all the information sources and literature used. This work, or a substantial part of it, has not been presented to obtain another or the same academic title.

Prague, 2018

Michal Kalus

Abstract

This Bachelor thesis dissertates about the influence of electromigration dispersion and Taylor dispersion to the total peak dispersion. Firstly, it deals with a solution to a new mathematical theory for peaks influenced by the EMD that was discovered in our research group and it experimentally proves the rightness of the solution. Specifically, it deals with comigration of two analytes with similar mobilities. Secondly, the goal was to find how the Taylor dispersion influences the separation process. This opens a way to further research on how these two effects collide and how they influence the system and separation process together.

Table of contents

Used shortcuts

CZE – Capillary Zone Electrophoresis

BGE – Background Electrolyte

EMD – Electromigration Dispersion

EOF – Electroosmotic Flow

TRIS – Tris(hydroxymethyl)aminomethane

DMSO – Dimethyl Sulfoxide Anhydrous

NAP - (S)-(+)-2-(6-Methoxy-2-naphthyl)propionic acid

FBP - (R)-(-)-2-Fluoro-α-methyl-4-biphenylacetic acid

v - Velocity

μ - Mobility

E – Electric Field Strength

μ_{app} – Apparent Observed Mobility

μ_{eff} – Effective Mobility

J - flux

j_{diff} – Diffusion Flux

D – Diffusion Coefficient

c – Concentration

f – Function

σ – Standard Deviation

σ^2- Variance

t – time

t_m – peak migration time

A – amplitude of peak

S_i – Relative Velocity Slope

K – conductivity

a_0 – Parameter of Peak Area

a_1 – Parameter of Gaussian Component

a_2 – Parameter of Standard Deviation Without Distortion

$a_{3\delta}$ – Parameter of Peaky Asymmetry

HVL_δ - Haarhoff-van der Linde Function

j_{mig} – Migration Flux

j_{con} – Convection Flux

φ – Potential

λ – Eigenvalue

$\vec{j}_c$ – Current Density Vector

Q - Charge

P - Pressure

R - Radius

η - Viscosity

L - Length

D_{eff} – Effective Diffusion Coefficient

k – Dispersion Coefficient

TD – Taylor Dispersion

t_{cor} – Corrected Time

t_{bc} – Time Before Correction

V – Volume

DE – Displacement Effect

TAE – Tag Along Effect

IS – Ionic Strenght

1. Theoretical introduction

1.1. Capillary zone electrophoresis

The capillary zone electrophoresis (CZE) belongs to a significant technical family whose principle is based on separation of charged compounds taking advantage of the fact that the migration velocity in an applied electric field depends on the size and charge of the molecule. The analytes move inside a narrow capillary tube filled with a background electrolyte (BGE), which allows the separation of various types of analytes, including small inorganic ions, different kinds of organic substances, and more complex biological macromolecules, such as proteins or amino-acids. In the CZE setup, the BGE is uniformly distributed along the capillary while a small sample plug of analytes is injected into the capillary. [1,2,3].

The movement of ions is defined by velocity, v, which is directly proportional to the electric field strength, E.

$$v = \mu \cdot E \tag{1}$$

This proportionality is characterized by the electrophoretic mobility, μ, dependant on the properties of the molecules as well as the solvent used.

The electroosmotic flow (EOF) is the movement of BGE caused by the electro-osmosis [4]. The observed (apparent) mobility, μ_{app}, of the analyte is determined by the combined effect of effective mobility and electroosmotic mobility [2,5].

$$\mu_{\mathrm{app}} = \mu_{\mathrm{eff}} + \mu_{\mathrm{EOF}} \tag{2}$$

After injecting the analytes and applying high voltage over the capillary, the analytes start to move towards the electrodes with different migration mobilities. For the setup where the cathode is at the outlet end of the capillary, the cations arrive at the detector first. The neutral particles are not influenced by the electric field, so they are carried only by the EOF mobility and they cannot be separated. For that reason, they are used for determining the EOF's mobility in the system, so-called EOF-markers. The anions arrive last because their effective mobility contributes negatively to the apparent mobility.

A pressure assisted CZE is a mode of CZE when a pressure difference is applied at the ends of the capillary along with an applied voltage. This introduces a pressure-driven flow in addi-

tion to the EOF. The pressure assisted CZE is used in order to make the separation faster or even possible, if the apparent mobility of the analytes is too small.

The detection is possible either on-column (on-line) or off-column (mass spectrometric or electrochemical)[6]. A record of a detector trace in electrophoresis is called electropherogram. The electropherogram provides information about the migration times of analytes and of EOF-marker.

1.2. Peak distortion in CZE

For many cases, the separation process is influenced by an effect that changes the ideal peak shape and causes distortion. The peak shapes can be dispersed and deformed or undergo diffusion. The effects that could influence the peak shape and cause the dispersion are [7,8]

A. Diffusion

The diffusion causes a symmetrical peak's broadening. For long migration time, the peak may disappear completely.

B. Electromigration dispersion (EMD)

The EMD is responsible for the nonlinear behaviour of peak shaping causing its triangular distribution.

C. Joule Heating and interactions with the capillary wall

Joule heating causes an increase in temperature in the capillary which influences the separation process by changing the chemical properties and it can cause that the separation does not occur. The interactions with the capillary wall cause the tailing which influences the migration time evaluation [7].

Out of these, this thesis focuses on diffusion and EMD.

1.2.1. Diffusion

If a concentration of a soluble substance in a fluid is not homogenous, the molecules of the substance move in streamlines until the concentration becomes homogenous in the whole fluid. This effect is called diffusion, and the movement is caused by thermal motion of particles. The velocity of the diffusion movement is governed by Fick's laws [9,10].

$$\vec{J}_{\text{diff}} = -D\frac{\partial c}{\partial x} \tag{3}$$

The diffusion flux, $\vec{J}_{\text{diff}}$, is the amount of matter n flowing through a unit area in unit time t. The diffusion causes the particles to move against the concentration gradient. Fick's first law states that the extent of the diffusive molecular flux is directly proportional to the concentration gradient with diffusion coefficient D being the coefficient of proportionality. This coefficient is characteristic of a given substance. Conditions that could influence the diffusion coefficient are the temperature and the solvent.

Fick's first law describes a flux under a steady-flow condition. The steady flow is a condition, when the diffusion flux remains constant during the whole process of diffusion (that means the concentration gradient remains constant). In reality, this assumption holds true only for an infinitely small interval since the diffusion flux naturally influences the spatial concentration distribution and hence the concentration gradient itself. Thus, the Fick's second law describes how the concentration changes with both time and space for a non-steady flow.

$$\frac{\partial c}{\partial t} = D\frac{\partial^2 c}{\partial x^2} \tag{4}$$

The diffusion occurs until the system reaches (dynamic) equilibrium, so there is no concentration gradient [11].

The injection plug in CZE can be approximated by a short rectangular plug. If nothing but diffusion occurs in the separation system, this injection plug profile results in a Gaussian peak shape after a certain period of time. The Gaussian peak shape is described by the normal distribution well known from mathematical statistics.

$$f_{(x)} = \frac{1}{\sigma\sqrt{2\pi}} e^{-\frac{(x-\mu)^2}{2\sigma^2}} \tag{5}$$

The normal distribution is defined by constant parameters, u and σ^2. The mean, u, is the average value describing the position of the normal distribution, and, σ^2 is the variance of the normal distribution. The shape of this function is called the "bell curve", its maximum is at $x = u$, and it is asymptotically approaching the x axe $\rightarrow \pm\infty$. It is symmetrical in its mean. The square root of the variance, $\sqrt{\sigma^2} = \sigma$, is called standard deviation. The width of a Gaussian peak, at any height, is a function of the standard deviation. At the base line, the width w equals to 4σ [12].

When the Gaussian peak passes through the detector it transforms into a time-dependent Gaussian function, with the amplitude of the peak A; peak migration time t_{m}; and standard deviation σ_t.

$$g(t) = Ae^{-\frac{(t-t_{\mathrm{m}})^2}{2\sigma_{\mathrm{t}}{}^2}} \tag{6}$$

It is desirable to have Gaussian peaks because they provide the highest detection sensitivity compared to other asymmetric peak shapes [13].

1.2.2. Electromigration dispersion

The EMD is caused by variations in the local conductivity. It causes characteristic triangular peak shape and is described by the relative velocity slope, where κ is the conductivity of the BGE, v is the migration velocity of the analyte and c is the concentration of the i-th analyte [14, 15].

$$S_i = \frac{\kappa}{v_i}\left(\frac{dv_i}{dc_i}\right)_{c_i \to 0} \tag{7}$$

For strong electrolytes it is possible to simplify the formula as follows [15]

$$S_i = \left(\frac{d\kappa_i}{dc_i}\right)_{c_i \to 0} \tag{8}$$

For weak electrolytes the EMD is influenced also by the dissociation of the analyte. In this case, a situation when the EMD is minimal even though the analyte changes the BGE conductivity markedly, is possible. Consequentially, there can also be a system where the EMD is strong even if the concentration of the analyte is minimal [16]. The result of electromigration dispersion is either a tailing peak ($S_i > 0$) or a fronting peak ($S_i < 0$) [1]. The EMD velocity profile is always the same across the capillary but differs along the capillary as we can see in *Figure 1*.

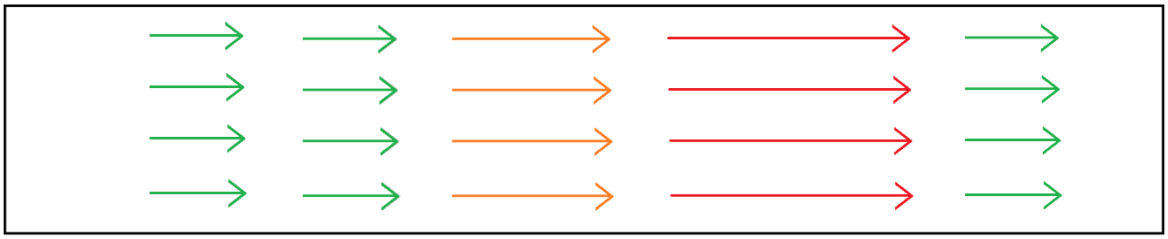

Figure 1 – The velocity profile of EMD (tailing peak, $S_i > 0$). The velocity in a zone varies along the capillary because of the changes in conductivity. Green lines are for the slowest velocity, red lines belong to the fastest velocity in the zone, while orange lines are the transition between slow and fast velocity

The problem that is caused by the EMD is that the migration time of these peaks is not readable directly from the electrophoretogram, simply because the time at peak maximum is not the real migration time because of peak deformation. Thus, to solve this problem the Haarhoff-van der Linde [17] function, which was originally created for non-ideal separations in HPLC, is used. It was also discovered that this function is an ideal fit for the peaks in capillary electrophoresis under influence of EMD. HVL is a universal function describing the Gaussian peak without EMD and a non-linear element which represents the EMD.

$$HVL_{\delta}(t) = \frac{\frac{a_0}{a_2 a_{3\delta}\sqrt{2\pi}} \exp\left[-\frac{1}{2}\left(\frac{t-a_1}{a_2}\right)^2\right]}{\frac{1}{\exp(a_{3\delta})-1} + \frac{1}{2}\left[1+\operatorname{erf}\left(\frac{t-a_1}{\sqrt{2}a_2}\right)\right]} \tag{9}$$

The four parameters describe the peak area a_0; the peak center a_1 of the Gaussian component which is equal to the migration time; the standard deviation of the peak as if it did not undergo a distortion a_2; the parameter $a_{3\delta}$ includes the effect of the EMD and diffusion, so it describes the asymmetry of the peak itself [18]. It can be shown that the HVL function is a natural solution of the continuity equations for CZE setup. Details will be discussed in the next section of this work.

1.3. Continuity equation in CZE

The continuity equation is an equation that explains how certain quantities are transported and preserved. The general form of the continuity equation then reads

$$\frac{\partial c_i}{\partial t} = -div\vec{J}_i \tag{10}$$

where $\vec{J}_i$ is the vector of the molecular flux of an i-th species at a certain location in the system, and c_i is a concentration at this location. The div operator stands for the divergence. In general, the vector $\vec{J}$ consists of three spatial components and is a function of each of spatial coordinates. The divergence is a sum of the partial derivatives of every spatial component of the vector with respect to the respective spatial coordinate. For the sake of simplicity, we will consider the system as one dimensional from here on. We can make such an assumption because in CZE the flows uniformly across the capillary. (This assumption is valid under neglecting a thin layer nearby the capillary wall.) This simplifies the equation (10) to

$$\frac{\partial c_i}{\partial t} = -\frac{\partial \vec{J}_i}{\partial x} \tag{11}$$

For CZE, the quantity we deal with is the particles concentration. The propagation of such concentration depends on three major influences that compose the total flux.

$$\vec{J} = \vec{J}_{\text{diff}} + \vec{J}_{\text{mig}} + \vec{J}_{\text{con}} \tag{12}$$

It says that the flux in capillary is a combination of diffusion, electromigration and convection. Convection is the movement caused by exterior forces (EOF, pressure, mixing, etc.)[19]. However, we do not need to consider the convection part in the equation (12) [20]. In case of a nonzero EOF or pressure (or any other constant) flow, we can compensate it by choosing a frame of reference moving along the x axis. Diffusion is described by the Fick's laws (7). Electromigration is an organized movement of particles due to electric force and the flux results as

$$\vec{J}_{\text{mig}} = -\frac{z}{|z|}\mu\, c\, \nabla\varphi \tag{13}$$

The factor $\frac{z}{|z|}$ indicates the direction of the migration of ions. The mobility μ, concentration c, and potential gradient $\nabla\varphi$ all influence the electromigration flux. The gradient operator ∇ can be described as a slope for function of N variables (it is a vector of first derivates of these variables).

By its definition, the potential gradient $\nabla\varphi$ equals to a negative intensity of electric field, E in one dimension. Thus, the electromigration term can be rewritten as

$$\vec{J}_{\text{mig}} = \frac{z}{|z|}\mu\, c\, \vec{E} \tag{14}$$

Further,

$$\vec{E} = \frac{\vec{J}_c}{\kappa} \tag{15}$$

Where $\vec{J}_c$ is a vector of current density and κ the (local) conductivity. The current density is constant vector along the capillary at a given time and has the direction of movements of cations. Consequently, we get

$$\vec{J}_{\text{mig}} = \frac{z}{|z|}\frac{\vec{J}_c}{\kappa}\mu c \tag{16}$$

Thus, for the total molecular flux, equation (12) in CZE becomes

$$\vec{J} = -D\frac{\partial c}{\partial x} + \frac{z}{|z|}\frac{\vec{J}_c}{\kappa}\mu c \tag{17}$$

and the continuity equation (11) becomes

$$\frac{\partial c_i}{\partial t} = \mathrm{D}_i\frac{\partial^2 c_i}{\partial x^2} - \frac{z}{|z|}\frac{\partial}{\partial x}\left(\frac{\vec{J}_c\mu_{i,eff}c_i}{\kappa}\right) \tag{18}$$

where the effective electrophoretic mobility of the i-th species $\mu_{i,eff}$ [21] is given as

$$\mu_{i,eff} = \sum_k \chi_k\mu_k \tag{19}$$

In equations (19) and (20), the index i refers to the i-th species and the index k (the maximum and minimum value of which differs for every i) refers to the k-th ionic form of that species.

χ_k stands for a molar fraction of the *k*-th ionic form with respect to the total amount of the *i*-th species (at a given place and time).

Then, the conductivity κ equals

$$\kappa = \sum_i \sum_{k(i)} c_k |z_k| \mu_k \tag{20}$$

Thus, the continuity equation for CZE describes the change of concentration of every chemical component in spatial and time coordinate. This leads us to a set of equations for each component. When solving the continuity equations for CZE, we reach the problem that the continuity equations are nonlinear. The conductivity term causes the nonlinearity of the system during the separation process, because it depends on the concentration of each analyte and on acid-base equilibria. Similarly, the effective mobility $\mu_{i,eff}$ is a function of local acid-base equilibria and may differ along the capillary for weak acidic or basic species.

The set of partial differential equations leads to a matrix problem [22], where the concentrations are grouped into a (column) vector $\vec{c}$ and the equations are summarised as

$$\frac{\partial c}{\partial t} = \mathbb{D}\frac{\partial^2 c}{\partial x^2} - \mathbb{M}\frac{\partial c}{\partial x} \tag{21}$$

The matrix $\mathbb{M}$ involves all the nonlinear terms involved in the migration fluxes $\vec{j}_{mig,i}$, which means that it generally depends on all the concentrations (but not their derivatives). The same applies to the diffusion fluxes $\vec{j}_{diff,i}$, with the exception that now the matrix $\mathbb{D}$ depends not only on all the concentrations but also on their derivatives with respect to x.

1.3.1. Linearization approach (by Štědrý)

With this approximation, we first neglect the diffusion fluxes $\vec{j}_{diff,i}$ (thus we effectively put the diffusion matrix $\mathbb{D} \equiv 0$) and we evaluate the matrix $\mathbb{M}$ at zero concentration of all analytes and concentrations of BGE components equal to the unperturbed BGE. Considering all these facts the matrix $\mathbb{M}$ becomes constant and can be diagonalized. The entire procedure loses all information about nonlinear effects in the system but leads to a set of continuity equations that are now decoupled. Additionally, the concentrations c_i have transformed into wave functions w_i on the way to the diagonal matrix. The wave functions are formed of linear combinations of the concentrations. Consequently N characteristic waves propagate through the system, where N is identical to the number of constituents, same as the number of concentrations c_i. The matrix $\mathbb{M}$ has N eigenvalues $\lambda_{0,i}$ that correspond to the velocities which the

waves propagate through the system with. It can be shown that for every analyte a corresponding wave function can be found that propagates with a velocity equal to the electrophoretic velocity of that analyte. The other wave functions correspond to the so-called system peaks that propagate through the system but do not belong to any analyte.

Diagonalization of matrix $\mathbb{M}$ reveals the existence of the wave functions and their velocities but do not allow to find a solution of their shapes (peak distributions). The problem has been solved by Hruška [20]. If we apply the Taylor expansion over both matrices $\mathbb{M}$ and $\mathbb{D}$ and consider only the constant term for the matrix $\mathbb{D}$ and the constant and the first nonlinear term for the matrix $\mathbb{M}$ (and evaluate them under the limit of zero concentrations of analytes), we arrive to a set of decoupled equations for the wave functions

$$\frac{\partial w_i}{\partial t} = -\frac{\vec{j}}{\kappa_{BGE}}\left(\lambda_{0,i} + \frac{\partial \lambda_i}{\partial w_i} w_i\right)\frac{\partial w_i}{\partial x} + \delta_i \frac{\partial^2 w_i}{\partial x^2} \tag{22}$$

where κ_{BGE} stands for the conductivity of the BGE, the term $\frac{\partial \lambda_i}{\partial w_i}$ is the first-order approximation of how the *i*-th eigenvalue of the matrix $\mathbb{M}$ changes with an increase in amplitude of the corresponding wave function, and the δ_i coefficient is the zero-order approximation of the diffusion coefficient of the *i*-th wave. The solution for this expanded linearized equation, if we consider the Dirac function as the initial condition, is the HVL function. This justifies using the HVL function as a first approximation to the peak distribution function in CZE.

The Dirac distribution is infinitely narrow, so if we consider the system with two or more analytes, the solution describes a situation in which they separate infinitely fast which keeps them from co-interacting. Thus, this solution cannot describe the system where two ions with similar mobilities migrate as analytes. To find a solution for such a system, Dvořák chose a different approach in his yet unpublished publication introduced during his ongoing doctoral studies in our research group.

1.3.2. Non-linear model (by Dvořák)

In contrast with Štědrý and Hruška [19, 20, 23], Dvořák's model returned to the fully nonlinear system, yet completely discarding the effect of the diffusion ($\mathbb{D} \equiv 0$). This model is described in yet not published publication that is under the preparation. He first shows that when analytes separate from the system zones, the wave functions of the analytes can be identified with their individual concentration distributions. Second, it was assumed that the molar fractions χ_k, equation (19), remain constant within the sample zone. This is fulfilled for strong electrolytes or under the constant pH conditions in the sample zone, equal to pH of the BGE.

The constant pH conditions are achieved for a small amount of sample migrating in a well-buffering BGE. Finally, the following set of quasilinear partial differential equations for the analytes was derived

$$\frac{\partial c_i(x,t)}{\partial t} + \frac{\partial}{\partial x}\left(\frac{v_i c_i(x,t)}{1 + \sum_{j=1}^{N_A} \frac{\kappa_j\left(\vec{C}^{\mathrm{BGE}}\right)}{\kappa_{\mathrm{BGE}}} c_j(x,t)} \right) = 0 \qquad (23)$$

where N_A is the number of analytes (out of the N constituents in the system) and κ_j is the contribution of the *j*-th analyte to the conductivity in its zone,

$$\kappa_j = \frac{\partial \kappa}{\partial c_j} \qquad (24)$$

For the injection of a rectangular sample distribution at $t = 0$, it is possible to find an analytical solution of these equations if the number of analytes is one or two.

While examining this solution, it is necessary to clarify the fact that the propagation of the analyte's concentration is not continuous, and we find discontinuities in concentration after some time after the initial injection. The discontinuity is called a shock. Since the diffusion term has been completely abandoned in this approach, the discontinuity manifests itself in a solution as an abrupt change in the concentration distribution, so the solution is only piecewise continuous.

For a single analyte, the propagation solution is a triangular peak shape (cf. *Figure 2 - D*) typical for the EMD as shown by Mikkers already in 1979 [24]. The following part describes the solution for the comigration of two analytes in nonlinear system which is newly introduced by Dvořák. The solution depends on the individual contributions κ_j of the two analytes to the local conductivity in their zone. It can be best demonstrated by the following schemes (*Figure 2*), that apply to a case where both contributions are positive, meaning that both analytes increase local conductivity compared to the BGE. Analogically to the chromatography [25], during the separation of two analytes with similar mobilities, we observe two kinds of distortion specific for both slower and faster analyte. The first effect is called the Displacement effect (DE), the second one is called the Tag along effect (TAE) [26].

The DE appears when the concentration profile of faster analyte is pushed forward by the concentration profile of slower analyte causing a formation of a specific concentration jump of faster analyte at the shock boundary between two analytes. This is the result of changes in conductivity caused by the presence of slower analyte – the conductivity of zone of faster analyte is below the value it would have had if it was sole. The decrease of conductivity is followed by the increase of velocity of the faster analyte zone which causes the DE – the concentration jump. Also, the more of slower analyte is at the beginning, the more the DE is pronounced.

The TAE is caused by the interaction of both concentration profiles in the region where they overlap. The slower analyte tags along with the faster one in this region and only slowly leaves it. The reason is the similar to the DE. In the part where they overlap, the conductivity decreases so the velocity of analyte is faster – slower analyte catches up with the faster one and that causes the TAE It also causes a creation of concentration plateau in the slower analyte zone.

In *Figure* 2, the sample zone is divided into several regions to describe the peak propagation in detail. *Panel A* shows the situation several seconds after the injection. In region *Y* the concentration of both analytes is zero. In region *T* we observe how the concentration of slower analyte grows, from the very zero concentration to the maximum (this maximum does not change in time). Until the very end of the separation, the concentration of slower analyte is constant in region *V* where it forms a plateau that is caused by TAE. This plateau widens from *Panel A* to *Panel B* and then, as we can see in Panel D, the plateau disappears after the two peaks are totally separated.

In region *S1*, both concentrations grow until they reach their initial concentration in region *Z*. For short period of time we can see also the concentration jump in region *X* where the concentration of slower analyte is zero while the concentration of faster analyte is far above the initial concentration.

However, region *Z* soon disappears, and region *S1* catches up the ending edge of region *S2* (that is the shock boundary S_{I}). Its fronting edge is other shock boundary, S_{II}. Across the first shock boundary S_{I}, there is a discontinuity in concentration of both analytes. Across the second shock boundary S_{II}, there is a discontinuity only for faster analyte, because S_{I} does not allow slower analyte to penetrate further. Regions *S1* and *T* broaden during the separation because their fronting edge moves faster than the slower ending edge.

At *Panel B*, it is possible to see that the DE occurs (region S2). A big part of faster analyte is pushed right at the fronting end of shock boundary S_I, caused by slower analyte's presence. The presence of slower analyte decreases the conductivity in region where they overlap, and it causes a huge jump of the faster analyte at this boundary.

After certain time, two peaks separate (P*anel C*). When all concentration of faster analyte penetrates through shock boundary S_I, this shock boundary is caught up by the region *T* and the plateau *V* also disappears and the peak of slower analyte is formed (*Panel D*).

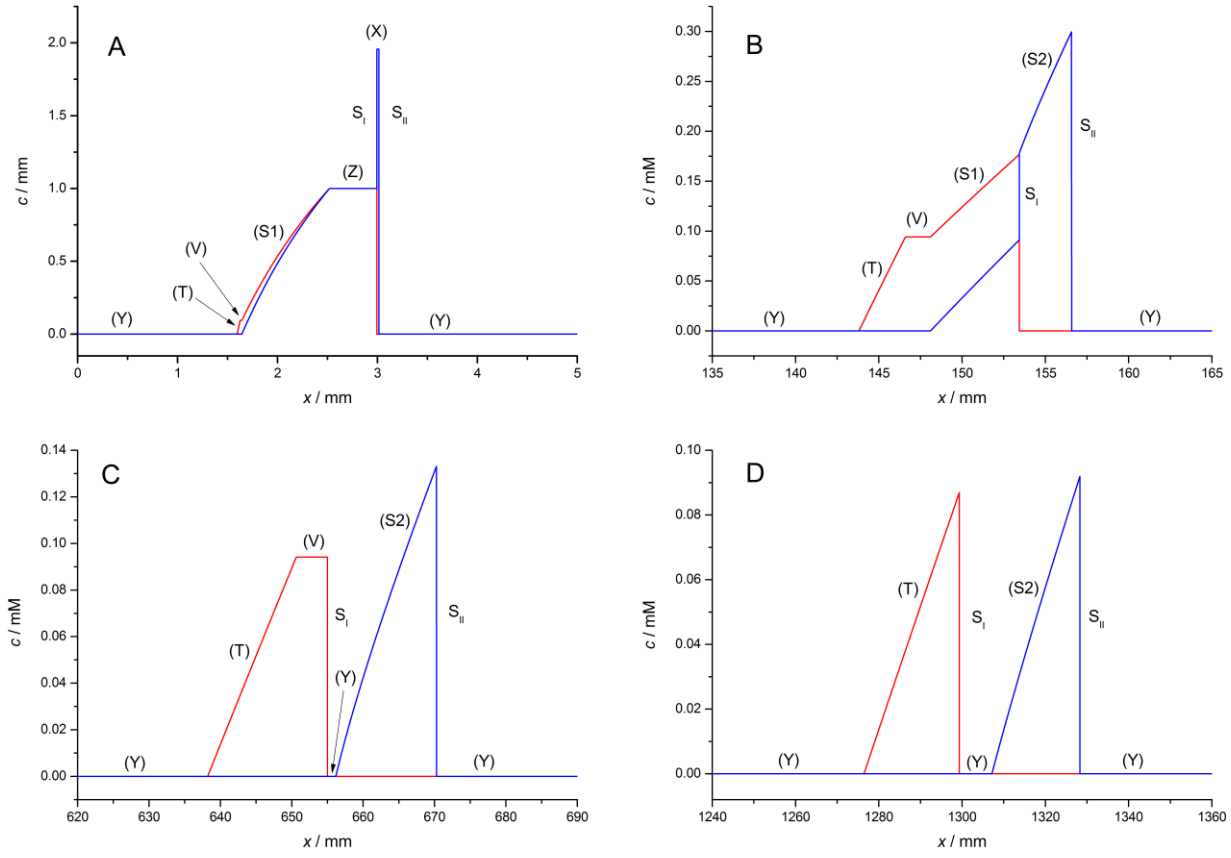

Figure 2 - The comigration and co-interaction of two analytes

1.4. Taylor dispersion and Taylor dispersion analysis

The laminar flow of an incompressible Newtonian fluid of certain viscosity, η, in a long horizontal cylindric tube (pipe) of length L, and radius $r << L$, under the pressure p, is called Poiseuille flow, described by Poiseuille' law as a volumetric flow rate, Q, [27].

$$Q = \frac{\Delta p \pi r^4}{8\eta L} \tag{25}$$

The solute that runs under Poiseuille laminar conditions is influenced by dispersion. The Poiseuille laminar flow velocity profile differs across the capillary but is the same along the capillary which we can see in *Figure 3*.

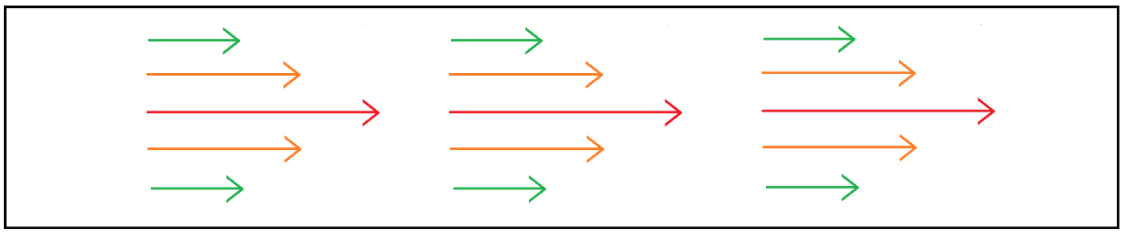

Figure 3 –Taylor dispersion velocity profile. The green lines represent the slowest velocity by the walls of capillary, the orange lines represent medium velocity and the red lines represent the fastest velocity, in the middle of capillary. This distribution of velocities forms a hyperbolic profile.

Since the velocity profile differs across the capillary, the simplification of the continuity equation (10) to one dimension cannot be adopted. Due to the cylindrical symmetry of the problem, the solution can be found in two dimensions if the Poiseuille laminar flow and the diffusion flux are the only two contributors to the vector of the molecular flux, $\vec{J}_i$. Interestingly, the result is that the solution is equivalent to yet again the one-dimensional continuity equation with an effective diffusion coefficient, called the dispersion coefficient,

$$k = D_{\text{eff}} = D\left(1 + \frac{u^2 r^2}{48 D^2}\right) \tag{26}$$

where D is the (molecular) diffusion coefficient of the solute and u is the velocity. The (equivalent) one dimensional continuity equation then results as

$$\frac{\partial c}{\partial t} = -v\frac{\partial c}{\partial x} + D_{eff}\frac{\partial^2 c}{\partial x^2} \tag{27}$$

where c is the cross-section average of the concentration and v is the cross-section average of the velocity. In other words, the solute under the influence of the Poiseuille laminar flow behaves as if the flow was not parabolic but uniform, but the solute has a higher diffusion coefficient that gives it a higher dispersion. This effect is called the Taylor dispersion (TD).

This dispersion is a combination of the radial diffusion of the molecules as well as convection. The convection is defined as axial spreading of the solute pulse along the direction of the flow. Because the fluid flows under Poiseuille laminar conditions, the velocity increases radially from a minimum at the walls to a maximum at the centre of the cylinder. The solute becomes more parabolic with time, and if there is no other dispersion influence, the solute will be increasingly dispersed over the length.

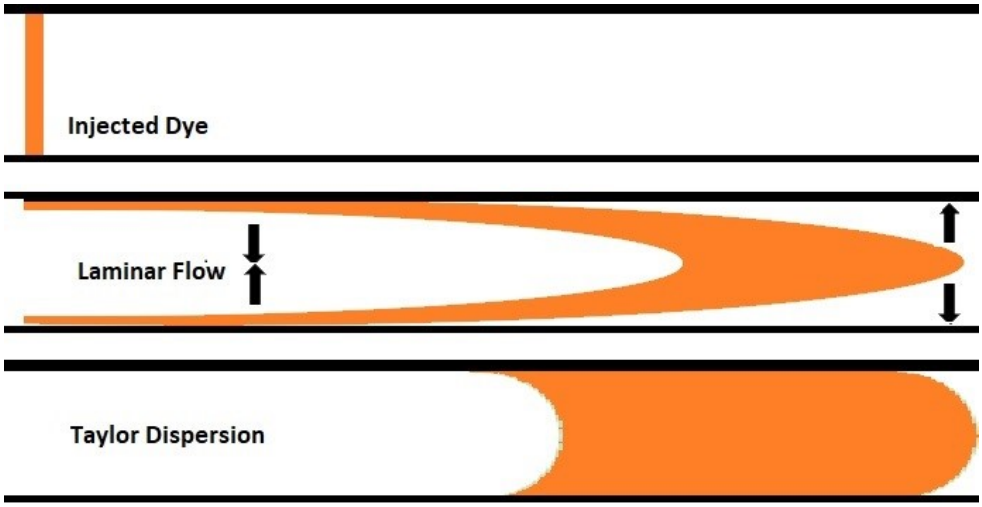

Figure 4 – Representation of propagation of the injected analyte under the Taylor Dispersion influence

Therefore, when the parabolic shape of the solute grows, the radial diffusion (perpendicular to the fluid flow) starts to occur. At the end of the solute pulse, the concentration of solute is higher at the walls, so the diffusion tries to move the molecules to the centre of the pulse where the concentration is lower. On the contrary, at the front of the solute pulse, the concentration of the solute is much higher at the centre of the pulse than at the walls, so the direction of the radial diffusion is opposite. Thus, though the diffusion is more often considered a spreading mechanism, in this case its role is the opposite. Hence, because of the radial diffusion the pulse is not spreading axially like it would with the convention influence only – the distribution is more compact [28].

The effect is used for Taylor dispersion analysis. The technique is used to detect and calculate the molecular diffusion coefficient through the concentration profile of dispersed sample. It is used in systems with microcapillaries where the solute is injected into the laminar flow of

running buffer while TD occurs. The variance σ^2 of the peak, see equation (5), is related to its initial variance ${\sigma_0}^2$, the diffusion coefficient D and time t.

$$\sigma^2 = {\sigma_0}^2 + 2Dt \tag{28}$$

After substituting the dispersion coefficient from equation (26) as the effective diffusion coefficient, we get the following relation.

$$\sigma^2 = {\sigma_0}^2 + 2t\left[D\left(1 + \frac{u^2 r^2}{48D^2}\right)\right] \tag{29}$$

This equation provides the relation between the TD, the molecular diffusion coefficient D and the peak's dispersion σ^2 after a time t it has spent in the laminar flow [29].

2. The objective of the thesis

The objective of this thesis can be divided into two main parts, both of which involve the phenomena that influences the peak shape in CZE.

The first one disserts on the confirmation of the new mathematical approach which deals with the description of comigration and non-linear co-interaction of two zones in the system influenced only by the EMD without the diffusion. The second one disserts about the Taylor dispersion's influence on the total peak's dispersion while using pressure during the experiment, so that the TD combines with the EMD. Neither of these effects has been described in the literature yet. The former study, the non-linear co-interaction of two zones, originates from the theoretical work of Martin Dvořák. For the latter, the EMD accompanied with the TD, an experimental and pseudo-experimental (computer simulation) basis is laid within this bachelor thesis with a prospect of continuation of the research in the longer run perspective.

The aims of the experiments are:

1. Experimental investigation of the theory of comigration and co-interaction of two ions.
2. a) Mathematical description of the influence of the Taylor dispersion on the peak shape without the Electromigration Dispersion.
   b) Computer simulation of relation between the Taylor dispersion and Electromigration Dispersion and their influence on the zone dispersion.

3. Experimental Part

3.1. Used Chemicals

All used chemicals were of analytical-grade purity.

Tris(hydroxymethyl)aminomethane (Tris), (S)-(+)-2-(6-Methoxy-2-naphthyl)propionic acid (S-NAP), (R)-(-)-2-Fluoro-α-methyl-4-biphenylacetic acid (R-FLU), dimethyl sulfoxide anhydrous (DMSO) were purchased from Sigma-Aldrich (Prague, Czech Republic). Hydrochloric acid (35 %) was purchased from Lachema a.s. (Brno, Czech republic). Sodium hydroxide for rinsing the capillary was purchased from Agilent Technologies (Waldbronn, Germany).

The water used for the preparation of all the solutions was purified by the Rowapur and Ultrapur water purification system (Watrex, San Francisco, USA). The IUPAC buffers, pH 7.000 and 9.012 (Radiometer, Copenhagen, Denmark), were used for calibration of the pH meter.

3.2. Instrumentation

The experiments were performed using ^{3D}CE apparatus for capillary electrophoresis (Agilent Technologies, Waldbronn, Germany) constructed with a built-in photometric diode array UV/VIS detector. For data analysis and control of the apparatus, ChemStation software (Agilent Technologies, Waldbronn, Germany) was used. A fused-silica capillary of 50 μm id and 375 μm od was provided by Polymicro Technologies (Phoenix, AZ, USA).

For all balancing we used the analytical balance Mettler AE 240 (Mettler Toledo, Switzerland), and for mensuration of pH we used a pH meter OHM 220 (Radiometer, Denmark) with combined glass electrode.

All solutions used in the experiments were filtered with syringe filters (Sartorius, Goettingen, Germany), pore size 0.45 μm and dissolved in an ultrasonic bath TranssonicDigitals TH075EL (Elma, Germany).

All data were evaluated and analysed in programs OriginPro 2016 (OriginLab, USA), CEval 0.6 [30] and MS Excel 2010 (Microsoft, USA). Simulations were performed in software PeakMaster 6 [31] and Simul 5 [32].

3.3. Experimental conditions

CE measurements were performed at temperature 25 °C, samples were injected hydrodynamically. The new capillary was flushed with deionized water for 10 minutes, then 5 minutes with 0.1 M sodium hydroxide, and then again for 5 minutes with deionized water.

Prior to each run, the capillary was flushed for at least 3 minutes with the relevant BGE. Each experiment was repeated at least three times.

3.3.1. Peak comigration experiments

The total length of the capillary and the length to the detector was 47.2 cm and 38.7 cm, respectively. The running buffer (BGE) was composed of 20 mM Tris and 10 mM HCl. Theoretical pH determined by PeakMaster 6 software was 8.12, experimental pH was 8.16.

S-naproxen (NAP) and R-flurbiprofen (FLU) were chosen as the analytes. The samples contained 1 mM analyte (FLU, NAP or mixture of both) dissolved directly in the running buffer and 0.04% DMSO as the EOF marker. Samples were injected hydrodynamically at 12×5 mbar s. The running voltage was 20 kV (cathode at the detector side). The analytes were detected at 220 nm and 250 nm.

The simulations in Simul 5 were run without the correction for ionic strength (IS). Effective mobilities for the respective IS were taken from the real experiment as input parameters, being $\mu_{\mathrm{NAP,eff}} = 20.799 \cdot 10^{-9}\ \mathrm{m^2V^{-1}s^{-1}}$ and $\mu_{\mathrm{FBP,eff}} = 20.575 \cdot 10^{-9}\ \mathrm{m^2V^{-1}s^{-1}}$. The EOF migration time was also chosen from the experiment, $t_{\mathrm{EOF}} = 2.3925$ min.

3.3.2. Taylor dispersion experiments

In first part, the samples were injected hydrodynamically at 10 × 5 mbar s. The variation of pressure was used: 7, 10, 15, 20, 25, 30, 40 and 50 mbar. The analyte was detected at 200 nm. The total length of the capillary and the length to the detector was 47.4 cm and 38.9 cm, respectively. 0.2% DMSO dissolved in pure water was used as the analyte.

In second part, the simulation was run with voltage 14 kV and length to the detector of 45 cm. BGE consisted of 10 mM ammonium and 20 mM acetic acid. The tested analytes were 1 mM potassium and lithium (with hydrochloride as counterion). For two of four simulations, pressure flow of 1 mm/s was applied.

4. Results and discussion

4.1.Peak comigration experiment

For the experimental evaluation of the introduced theory it was necessary to find two analytes with very similar mobilities, so their migration times would be close to each other. This would cause that they co-migrate for long period of time, and the co-interaction of these two analytes occurs in efficient time, so it is possible to observe their behaviour while they pass through the detector. For these reasons, NAP and FBP were chosen.The limiting ionic mobility of NAP is $\mu_{\mathrm{NAP}} = (25 \pm 1) \cdot 10^{-9}\,\mathrm{m^2V^{-1}s^{-1}}$ $(\mathrm{pK_A} = 4.33 \pm 0.01)$ and the limiting ionic mobility of FBP is $\mu_{\mathrm{FBP}} = (24.5 \pm 1) \cdot 10^{-9}\,\mathrm{m^2V^{-1}s^{-1}}$ $(\mathrm{pK_A} = 4.19 \pm 0.01)$ [33]. Because their mobilities are similar and the EOF is quick (pH =8.16), the separation process is not finished before they pass through the detector. The experiment was executed for each analyte separately. Then, a mixture of both analytes was injected. The results were then compared with the computer simulation done by Simul 5 [32] and with the theoretical calculation according to the nonlinear theory by Dvořák. In *Figure 5,* we can see the experimental electropherograms.

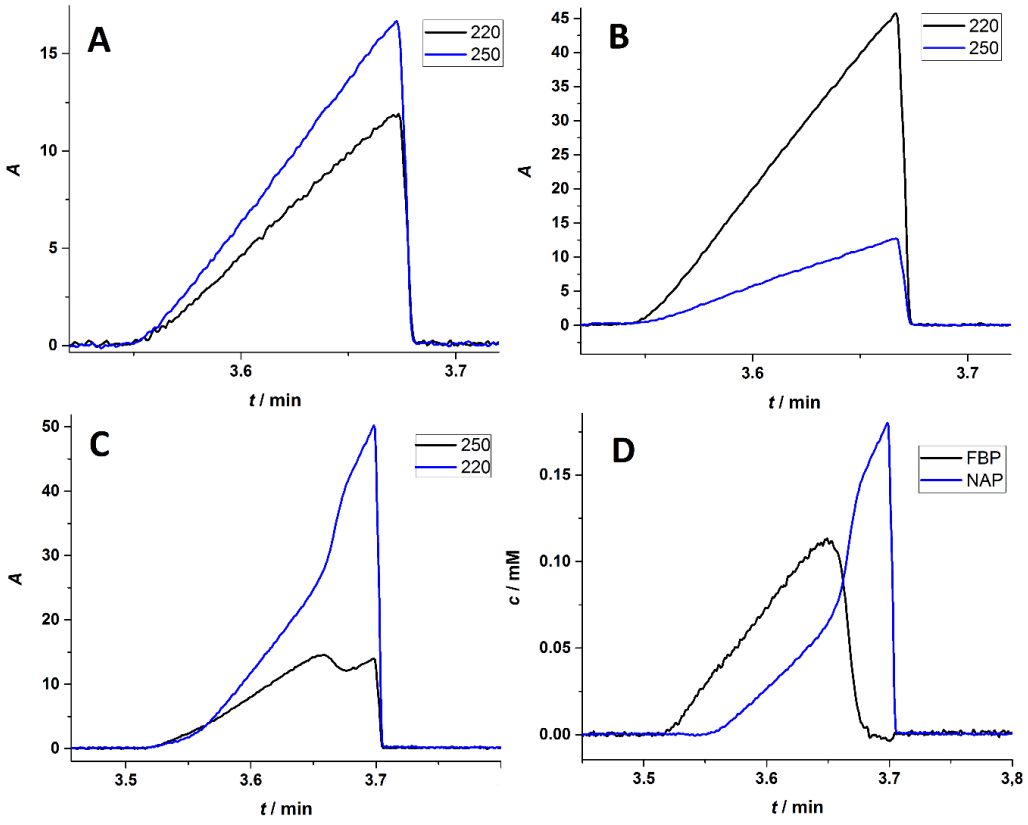

Figure 5 – Experimental data gathered for 220 nm and 250 nm for FBP (Panel A), for NAP (Panel B) for both analytes (Panel C) and linear combination of the two respective wavelengths for both analytes (Panel D).

The *panel A* represents the electropherograms for FBP for two wavelengths, 220 nm and 250 nm. It is possible to observe that the peak is influenced by the EMD and it has fronting shape – it creates a shock boundary at its front-end. The absorbance is different for each wavelength, for 250 nm being slightly smaller.

The *panel B* represents the electropherograms for NAP also for the two wavelengths, 220 nm and 250 nm. The peak shape is also fronting, but the difference in absorbance for each of wavelengths is more significant than for the previous analyte. Also, while FBP absorbs more at 250 nm, NAP absorbs more at 220 nm. It is convenient to notice that the migration times of both analytes are almost the same. The effective mobilities for these conditions are $\mu_{\mathrm{NAP}}{}^{*} = 20.799 \cdot 10^{-9}\ \mathrm{m^2V^{-1}s^{-1}}$ and $\mu_{\mathrm{FBP}}{}^{*} = 20.575 \cdot 10^{-9}\ \mathrm{m^2V^{-1}s^{-1}}$. These mobilities were then used as input data for simulation.

The *panel C* shows the electropherograms of both analytes for both wavelengths. It is possible to see the big difference in shape of peak for each wavelength. Both analytes absorb at both stated wavelengths (although the absorbance differs). Because of that, the data were processed mathematically to obtain the individual contribution of each analyte (*panel D*).

We work with all three previous measurements. Single analyte measurements of FBP and NAP and both analytes measurement. The results were modified by adjusting the time axis to counterbalance the difference in EOF times of each measurement. This way the position of peak on time axis can be unified. Nevertheless, the amount of time the peak spends in capillary cannot be changed. This fact might cause a problem in case when the EOF velocity differs significantly. That is, however, not this case. For this system, the EOF times were $t_{\mathrm{eof,FBP}} = 2.4058\ \mathrm{min}$, $t_{\mathrm{eof,NAP}} = 2.3925\ \mathrm{min}$ and for the sample of both analytes $t_{\mathrm{eof,both}} = 2.3958\ \mathrm{min}$. It is possible then to neglect the differences in EOF velocity.

For the recalculation, the following equation was used.

$$t_{\mathrm{cor}} = \frac{1}{\left(\frac{1}{t_{\mathrm{bc}}} - \frac{1}{t_{\mathrm{EOF}}} + \frac{1}{t_{\mathrm{rEOF}}}\right)} \tag{30}$$

The time t_{cor} represents the time after the correction, the time t_{bc} represents the time before the correction. The times t_{EOF} and t_{rEOF} represent the time of EOF in the experiment performed at 220nm, and for the simulation, respectively.

Then, it is evident that for FBP, the absorbance at 250 nm is 1.36-times higher than at 220 nm. For NAP, the absorbance at 220 nm is 3.54-times higher than at 250 nm. From this we obtain the following set of equations.

$$\text{I. } A_{250} = 1.36c^*_{\mathrm{FBP}} + 1c^*_{\mathrm{NAP}} \tag{31}$$

$$\text{II. } A_{220} = 1c^*_{\mathrm{FBP}} + 3.54c^*_{\mathrm{NAP}} \tag{32}$$

A_{250} and A_{220} are the absorbances for respective wavelengths. c^*_{NAP} and c^*_{FBP} are the pseudo-concentrations of our analytes that are proportional to the real concentrations. As solution of set of equations for each point of time axis, we receive the decomposition of two signals (250 nm and 220 nm). In *Panel D,* it is possible to see the corresponding profiles of both analytes. After that, the resulting picture allows to compare the experimental data directly to simulation and the mathematical model because the peak areas become identical. In this panel, we also observe the peculiar peak shape of two comigrating analytes. Even though their mobilities are similar, and the peak shapes of both analytes are similar when they migrate alone, for the comigration we observe that the slower analyte, that is FBP, pushes the faster one, NAP, to the front-edge and causes the shock boundary to rise. We observe that the Tag along effect and the Displacement effect both take place in calculated diagram as was expected from the theory.

Next, we ran a simulation in Simul 5. *Figure 6* shows the result of the simulation (record from the detector) compared to the data from panel D. We observe that the contribution of FBP calculated from the experiment is in very good agreement with simulated data. The migration time of the shock boundary of NAP zone is slightly higher for the experiment; the concentration profile of NAP is lower and wider as if the separation process took longer than in the simulation. Since the whole peak is wider, the height is naturally lower to preserve the peak area. It can be caused by the fact the injection of the sample in the experiment can be inaccurate (therefore, we do not know the exact length of the injection zone which is one of input parameter to the theory). However, the profiles correspond qualitatively (all the effects can be observed in both cases).

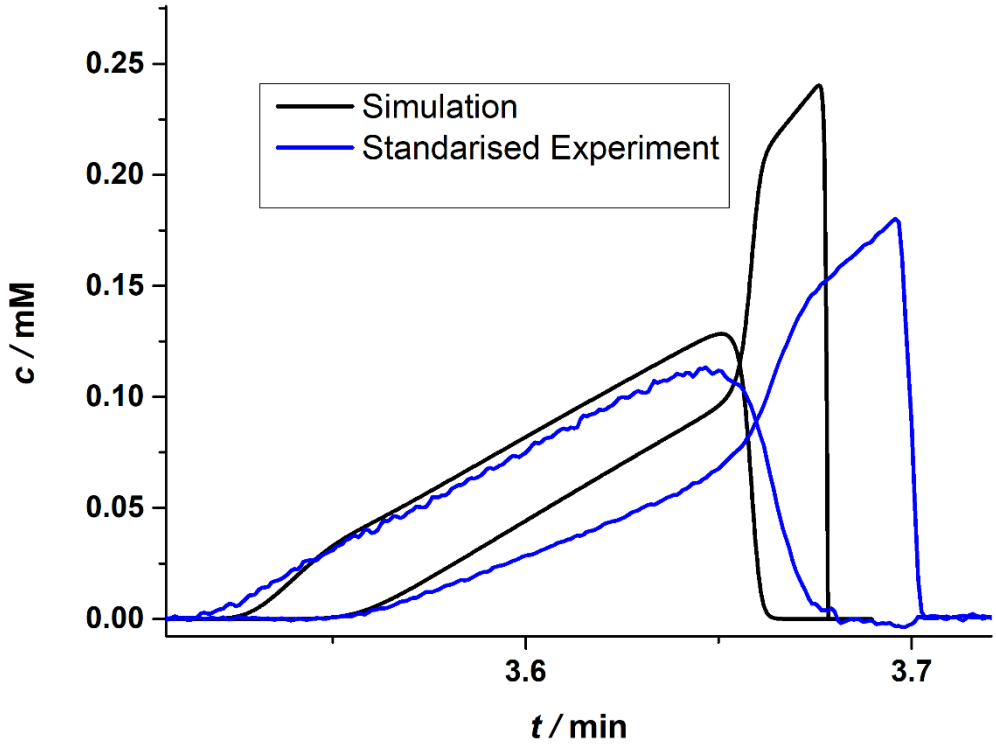

Figure 6 - Comparison of experimental and simulated data. The blue lines represent the decomposition of the original signals (220 nm and 250 nm) according to set of equations (31-32). The black lines represent the simulation data. The first peak upon the detector is FPB, second is NAP.

The real-time simulation was then compared to the non-linear model calculation (*Figure 7*). It was necessary to move the x-axis of simulation so that the peak starts at 0 mm and ends at 1.08 mm. Because in simulator the middle of the peak is placed at 10 mm, the x-axis was moved for 9.46 mm.

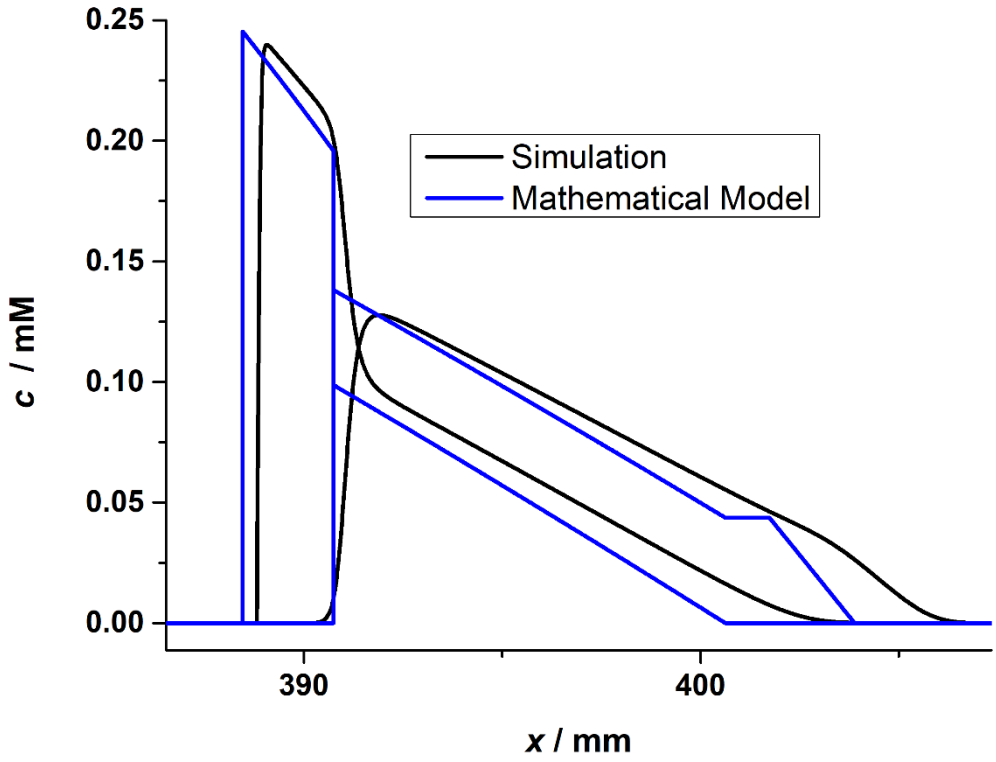

Figure 7 - Comparison of mathematical and simulated data. The blue lines represent the nonlinear model (without the diffusion). The black lines represent the real-time simulations (with diffusion's influence).

In the real system (and for simulation) we cannot neglect the diffusion, so the peak shape undergoes more broadening and the boundaries are smoother. It is possible to see that the plateau at the front end of mathematical model almost disappears when the diffusion takes place, however it is still possible to see the effect. The diffusion might also cause that the tail of FBP is longer for the simulation than for the mathematical model. Also, the shock boundary is more perpendicular for the mathematical model than for the simulation data, which is also caused by the diffusion. Still, both characteristic effects can be observed very well, and the predicted co-interaction of both analytes was successfully proved.

For conclusion, the theory of Dvořák was successfully compared to experiment and simulation. Slight difference can be caused by external effects like diffusion or by the process of standardisation. However, the mathematical model and simulations are well comparable to the experimental data.

4.2. Taylor dispersion experiments

4.2.1. DMSO experiment

In the first part, our interest was to find how the TD alone influences the separation process and the total peak shape dispersion, respectively. In the experiment, different pressures were used to find out how the peak shape changes and determine the diffusion coefficient of DMSO from the dependence, if possible. The sample consisted of 2% DMSO and was dissolved in water. Then, it was pushed through the capillary to the detector using different pressures. The whole scale of pressures from 7 mbar to 50 mbar was applied. The respective electropherograms can be seen in *Figure 8.* It is possible to see that the detection times (the term "migration time" is not used here since there is no electromigration) decrease with increasing pressure. On the contrary, the broadening of peaks gets visually more significant with decreasing pressure. That could signify that the variance of peaks and the pressure are inversely proportional. However, that is not true as follows from the theory (33-39) and as we will see further.

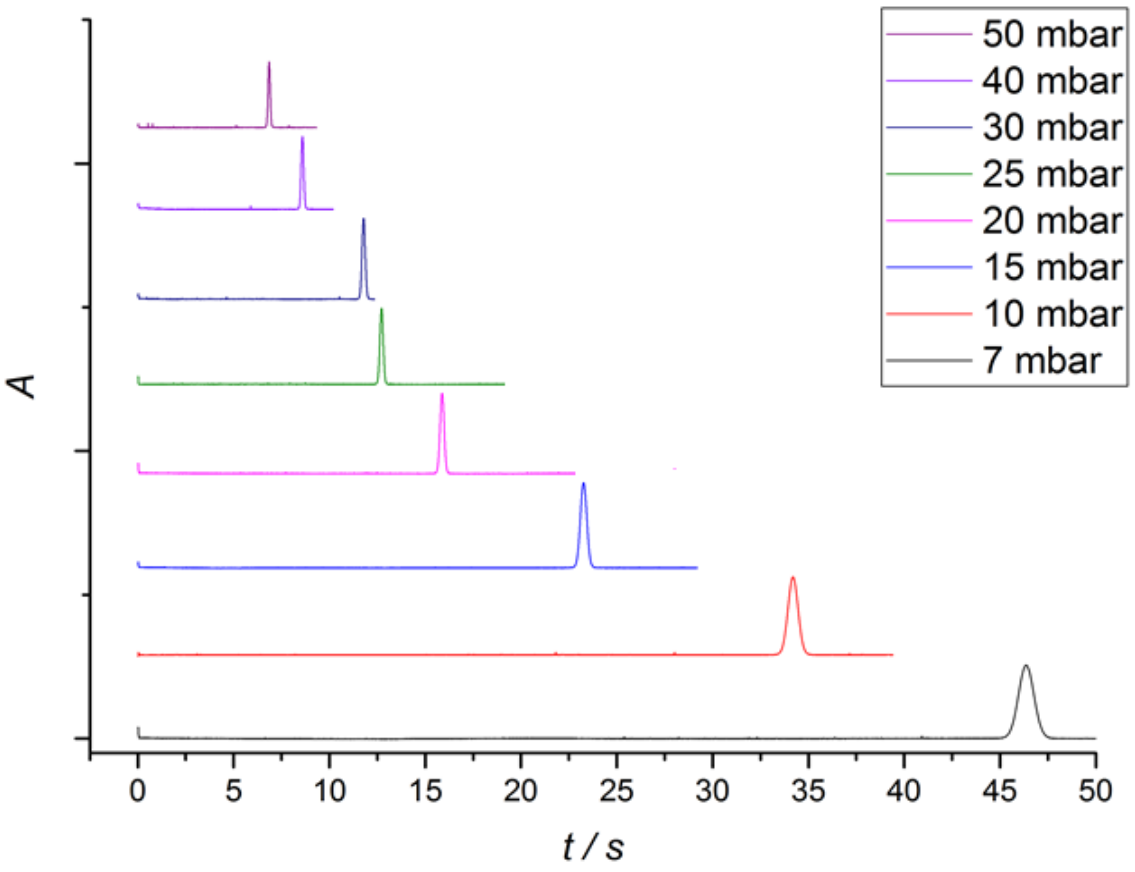

Figure 8 – Experimental electropherograms for different pressures; DMSO was used as the analyte. The preassure is decreasing from the upper part to the lower part.

The values of standard deviation, σ, were gained from the CEval 0.6 software [30]. Variance, σ^2, was calculated. Then, the values of variance were plotted against the migration times of the peaks. The obtained dependence is shown in *Figure 9*. This diagram shows how the variance changes over time (and with the pressure as well, because the pressure is indirectly proportional to time).

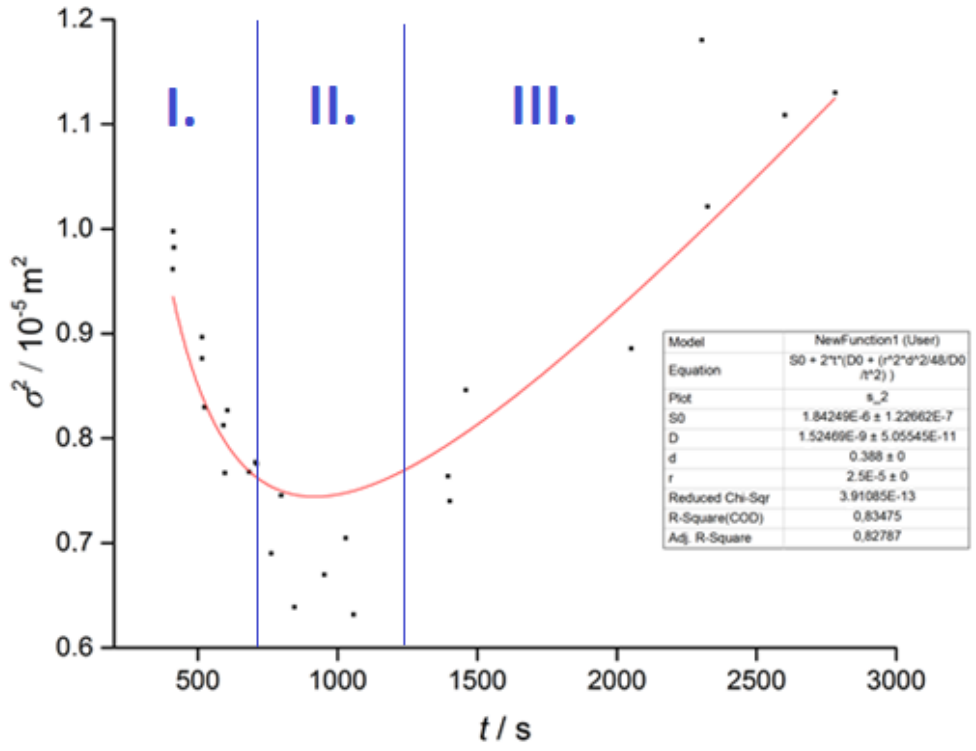

Figure 9 - The dependence of variance of the peaks (for different running pressure) on time.

The following equation was used for fitting the data that were measured.

$$\sigma^2 = {\sigma_0}^2 + 2t\left[D + \frac{{l_{\mathrm{det}}}^2 r^2}{48Dt^2}\right] \tag{33}$$

From the equation of Poiseuille flow (25), it is possible to derive the time, *t,* from volumetric flow, *Q,* as

$$\frac{V}{t} = \frac{\Delta p \pi r^4}{8 \eta l_{det}} \tag{34}$$

where V is a volume. Then, the equation is modified to a form

$$t = \frac{8 \eta l_{det} V}{\Delta p \pi r^4} \tag{35}$$

From the relation

$$V = l_{tot} \pi r^2 \tag{36}$$

it is possible to further derive the equation

$$t = \frac{8 \eta l_{det} l_{tot}}{\Delta p \pi r^2} \tag{37}$$

We can substitute the time in equation (33) with (37) to obtain

$$\sigma^2 = {\sigma_0}^2 + 2t \left[D + \frac{\Delta p^2 r^6}{3072 \eta^2 L^2 D} \right] \tag{38}$$

After modification, we receive the final form of the equation

$$\sigma^2 = {\sigma_0}^2 + \left[\frac{16 \eta l_{det} l_{tot} D}{\Delta p r^2} + \frac{\Delta p \, r^4}{192 \eta l_{tot} D} \right] \tag{39}$$

The equation in this form suits us to describe how the particular terms contribute to the function shape.

We can divide the dependence in Figure 8 to three regions. In region I, the variance of the analyte sharply grows with reducing time. In this region, the TD is much stronger than the diffusion, so the variance grows in a way that is limiting in $+\infty$ for time approaching zero. When the pressure is big, the term $\frac{\Delta p^2 r^6}{3072 \eta^2 L^2 D}$ in equation (38) is bigger than the diffusion coefficient D, so the growth of the curve is determined by pressure and the diffusion coefficient can be neglected (the diffusion influences the analyte for short time only). It is important to mention that for big pressures the approximations used for the equation derivation are not valid anymore.

In region II, the value of variance is at its minimum. This minimum occurs when the contributions of TD and diffusion are both minimal. The dispersion due to diffusion grows with increasing time and due to TD with decreasing time and increasing pressure, respectively. Mathematically, neither of terms $\frac{\Delta p^2 r^6}{3072\eta^2 L^2 D}$ and D can be neglected, and both contribute to the curve. Since the diffusion coefficient cannot be changed, but we can change the used pressure, it might seem that with this relation we can predict the best conditions for the separation process.

In region III, the pressure is minimal, so its contribution is negligible, and the main contribution is the diffusion. From equation (38), it is possible to see that for small pressures, the equation can be simplified to form (28), as if no TD was present because the term $\frac{\Delta p^2 r^6}{3072\eta^2 L^2 D}$ approaches 0. The diffusion is influencing the peak for significant time period, so the variance is again starting to grow. The function growth is not as sharp as in first region.

The main goal of this experiment was to prove that the measured dependence is in agreement with the function we derived (33). The curve in *Figure 9* has the expected shape, so the experiment may be considered successful. However, the measured value of diffusion coefficient of DMSO was $D_{DMSO,exp} = 1.52468 \cdot 10^{-9} \pm 5.05545 \cdot 10^{-11}\ m^2 s^{-1}$. This value is not consistent with other values found in literature. The diffusion coefficient of DMSO measured by NMR in water at 25°C was $D_{DMSO,1} = 0.730 \cdot 10^{-9}\ m^2 s^{-1}$ [34]. The other value of $D_{DMSO,2} = 0.88 \cdot 10^{-9}\ m^2 s^{-1}$ came from the molecular dynamics simulation [35]. Both values are approximately two times smaller than the data measured in this experiment.

For conclusion, mathematical function that describes the Taylor dispersion in CZE was successfully fitted to real experimental data. This function shows a trend that could lead to better separation conditions. On the other hand, the measured value of diffusion coefficient of DMSO was not in agreement with the values found in literature. Further research is needed to explain the difference.

4.2.2. 2D Simulations

In the second part, the 2D simulations to compare the contribution of the two effects – the TD and the EMD – were run. The simulations were contributed by Dr. Pablo A. Kler from National Scientific and Technical research Council in Santa Fe, Argentina. He cooperates with our group and is an author of a home-made 2D and 3D simulator for electrophoresis.

The ions of potassium and lithium were chosen because they are simple ions with well-known behaviour and well defined. Their physical and chemical behaviour is similar.

Simulated electropherograms can be seen in *Figure 10* and *Figure 11*. The detector trace was recorded at given position of the capillary as a concentration integral across the capillary.

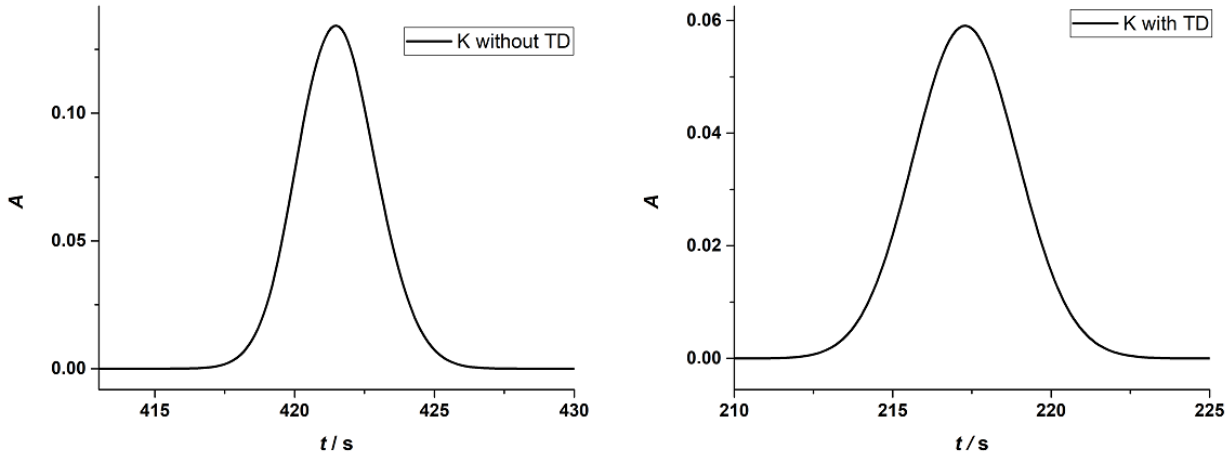

Figure 10 – The left image represents the propagation of potassium in CZE without the pressure applied (there was only EMD), the right image represents the case when the pressure was applied (there were EMD and TD influencing the system)

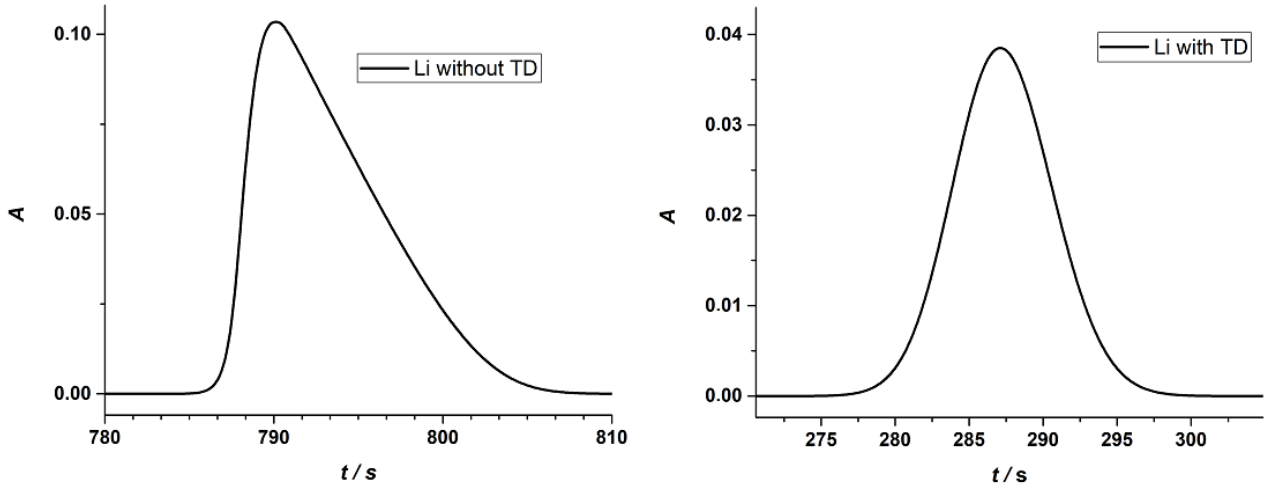

Figure 11 - The left image represents the propagation of lithium in CZE without the pressure applied (there was only EMD), the right image represents the case when the pressure was applied (there were EMD and TD influencing the system)

It is possible to see a trend between the simulation with and without pressure used. The peaks are not Gaussian when the pressure is not applied, they have tailing shape caused by the EMD

and their migration times are higher. When the pressure is applied, the peaks become more Gaussian and broadened. The migration times decrease significantly, for potassium the migration time decreases twice, for lithium thrice. It can be concluded that the TD has a significant contribution to the peak shape.

In BGE that we used in the simulation, the ammonium cation serves like a co-ion to ion of analyte. Next, the potassium cation has a mobility practically identical to ammonium cation. Thus, the EMD should not be manifested. On the other hand, the lithium cation is significantly slower than ammonium cation, that is why the EMD in this case is significant as well. Therefore, the change of peak shape is more significant in case of lithium cation.

When there is only EMD present, the peaks can be described by HVL function. For HVL, there is a parameter a_2 that equals to a standard deviation of Gaussian component of the peak as if no EMD was present. The values of this parameter and of other HVL parameters are stated in Table 1 (CEval 0.6 [30] was used to obtain the data, fitting the peaks with HVL equation). Then, the same procedure was applied to systems with TD, they were also fitted with HVL equation and the values of the regression parameters are also stated in *Table 1*. All the parameters were then compared.

	a_0 / A.s	a_1 / s	a_2 / s	$a_{3\delta}$ -
K (TD)	0.24195	217.4	1.6348	0.18728
K (no TD)	0.47033	421.77	1.3935	0.61073
Li (TD)	0.3171	287.8	3.2974	0.52853
Li (no TD)	0.90323	800.56	2.5993	13.569

Table 1 – Parameters of peaks representing the peak shape defined by HVL equation.

From *Table 1* it is notable that the parameter a_2 that describes the standard deviation without the influence of EMD is higher for the system where the pressure is applied – the peaks are more broadened. For potassium ion, the change in parameter a_2 is $\Delta a_{2,\mathrm{K}} = 0.2413$ when the pressure is applied. For lithium ion, the change in parameter a_2 is much higher, $\Delta a_{2,\mathrm{Li}} = 0.6981$.

If the parameter $a_{3\delta}$ that includes the effect of EMD is compared, there is bigger difference in its values for these two systems than for parameter a_2. Also, the parameter gets smaller after the pressure is applied – the peak shape becomes more Gaussian. For potassium ion, the

change in parameter $a_{3\delta}$is $\Delta a_{3\delta,\mathrm{K}} = -0.42345$ when the pressure is applied. For lithium ion, the change in parameter $a_{3\delta}$ is $\Delta a_{3\delta,\mathrm{Li}} = -13.04047$.

Out of this information, it is possible to conclude that the parameter $a_{3\delta}$, that includes the EMD component and its contribution to the peak shape, changes more than the parameter a_2, especially if the distortion in the system without the pressure is significant (case of lithium ion). This can lead to the assumption that the TD has significant influence on Gaussian peak shape. The difference in values between two ions can be caused by the ion size or different migration times. The change of the parameter is also more significant when the distortion in a non-pressure system was more relevant. The simulation needs to be proved experimentally and we need more data to make any conclusion. However, it is already possible to notice a trend that can be further studied and verified.

Conclusion

This thesis had two parts with three main goals that were successfully fulfilled. Both parts dissertated about the non-linear effects influencing the separation process in capillary zone electrophoresis.

Experimental investigation of theory of comigration and co-interaction of ions was successfully finished. The experimental measurements of comigration of NAP and FBP proved the mathematical model introduced by Dvořák accompanied by the simulated data that were also in line with the mathematical model. It was proved that the mathematical model is correct and that the real experiment behaves as predicted.

Mathematical description of the influence of Taylor dispersion on the peak shape when applying pressure was confirmed by the experimental measurements of DMSO in water. The trend between the applied pressure and variance of the peak was explored and the diffusion coefficient of DMSO was evaluated from the dependence. The value of obtained DMSO diffusion coefficient was in agreement with the values from literature [34, 35].

Computer simulations that aimed to explore the Taylor dispersion's and electromigration dispersion's mutual influence on zones were run in cooperation with Dr. Pablo A. Kler. It was found that the Taylor dispersion influences the peak shape significantly, leading to more gaussian shape when the pressure is applied. The electromigration distortion effect diminishes with the Taylor dispersion taking place. However, the research needs more data and it is expected that the study of this problem will continue.

Acknowledgment

I would like to express my special thanks to my supervisor Mgr. Magda Dovhunová who supported me, understood me and taught me many things the way others would not have been able to accomplish. My thanks also belong to Mgr. Pavel Dubský, PhD and the whole group in which I could do this thesis and research.

I would also like to thank my parents for many opportunities and support they gave me, as well as my friends – without them this thesis would be a way harder to accomplish.

Reference:

(1) Whatley, H. *Basic Principles and Modes of Capillary Electrophoresis*; **2001**.
(2) Kašička, V., *Chem. Listy,* **1997,** 91, 320–329**.**
(3) Whatley, H.; Humana Press Inc, Totowa, NJ, **2001**.
(4) Gordon, M. J.; Huang, X.; Pentoney, S. L.; Zare, R. N.; *Science* **1988**, *242* (4876), 224–228.
(5) Xu, Y. Tutorial: Capillary Electrophoresis. *Chem. Educ.* **1996**, *1* (2), 1–14.
(6) Swinney Kelly; Bornhop Darryl J; *Electrophoresis,* **2000**, 21, 1239–1250.
(7) Lunte, S. M.; Radzik, D. M.; *Progress in Pharmaceutical and Biomedical Analysis*; **1996**; 2, 3–21.
(8) Gaš, B.; Štědrý, M.; Kenndler, E.; *Electrophoresis,* **2005**, 18, 2123–2133.
(9) Tyrrell, H. J. V; *J. Chem. Educ.,* **1964**, 41 (7), 397.
(10) Poirier, D. R.; Geiger, G. H.; *Transport Phenomena in Materials Processing*; **2016**, 419–461.
(11) Macdonald, D.; *Transient Techniques in Electrochemistry*; **1977**, 47–67.
(12) James, F. *Statistical Methods in Experimental Physics*; **2006**.
(13) Wahab, M. F.; Patel, D. C.; Armstrong, D. W.; *J. Chromatogr. A* **2017**, 1509, 163–170.
(14) Gaš, B.; Kenndler, E.; *Electrophoresis* **2000**, 21 (18), 3888–3897.
(15) Gebauer, P.; Boček, P.; *Anal. Chem.* **1997**, 69 (8), 1557–1563.
(16) Chen, Z.; Ghosal, S.; *Bull. Math. Biol.* **2012**, 74 (2), 346–355.
(17) Erny, G. L.; Bergström, E. T.; Goodall, D. M.; Grieb, S.; *Anal. Chem.* **2001**, 73 (20), 4862–4872.
(18) Dubský, P., Dvořák, M., Műllerová, L., Gaš, B.; *Electrophoresis* **2015**, 36 (5), 655–661.
(19) Riesova, M., Hruška, V., Gaš, B.; *Electrophoresis***, 2012**, 33 (6), 931–937.
(20) Hruška, V., Riesová, M., Gaš, B. ; *Electrophoresis,* **2012**, 33 (6), 923–930.
(21) Tiselius, A. In *Nova Acta Regiae Soc Sci Ups*; Ser IV 7; **1930**; Vol. 4, pp 1–107.
(22) Poppe, H.; System Peaks and Non-Linearity in Capillary Electrophoresis and High-Performance Liquid Chromatography. *J. Chromatogr. A* **1999**, *831* (1), 105–121.
(23) Štědrý, M., Jaroš M., Hruška, V., Gaš, B.; *Electrophoresis***, 2004**, 25, 3071–3079.
(24) Mikkers, F. E. P.; Everaerts, F. M.; Verheggen, T. P.; , *J. Chromatogr. A,* **1979**, 169, 1–10.
(25) Guiochon, G.; Golshan Shirazi, S.; M Katti, A. *Fundamentals of Preparative and Nonlinear Chromatography / Georges Guiochon, Sadroddin Golshan Shirazi, Anita M. Katti*; **2018**.
(26) Golshan-Shirazi, S.; Guiochon, G.; *Chromatographia* **1990**, 30 (11), 613–617.
(27) On the Dispersion of a Solute in a Fluid Flowing through a Tube. *Proc. R. Soc. Lond. Ser. Math. Phys. Sci.* **1956**, 235, 67.
(28) Conditions under Which Dispersion of a Solute in a Stream of Solvent Can Be Used to Measure Molecular Diffusion. *Proc. R. Soc. Lond. Ser. Math. Phys. Sci.* **1954**, 225 (1163), 473.
(29) Felder, C.; Oltean, C.; Panfilov, M.; Buès, M.; *Comptes Rendus Mécanique,* **2004**, 332 (3), 223–229.
(30) Dubský, P.; Ördögová, M.; Malý, M.; Riesová, M. *Electrophoresis*; **2016**; 1445.
(31) Jaros, M.; *PeakMaster – A Freeware Simulator of Capillary Zone Electrophoresis*; **2005**.
(32) Hruška, V.; Jaroš, M.; Gaš, B.; *Electrophoresis,* **2006**, 27, 984–991.
(33) Riesová, M.; Svobodová, J.; Ušelová, K.; Tošner, Z.; Zusková, I.; Gaš, B.; . *J. Chromatogr. A* **2014**, 1364, 276–288.
(34) Holz, M.; Heil, S. R.; Sacco, A.; *Phys. Chem. Chem. Phys.* **2000**, 2 (20), 4740–4742.
(35) Vishnyakov, A.; Lyubartsev, A. P.; Laaksonen, A.; *J. Phys. Chem. A* **2001**, 105 (10), 1702–1710.